CHEMICAL PHYSICS

Fifth-order time-domain Raman spectroscopy of photoactive yellow protein for visualizing vibrational coupling in its excited state

Hikaru Kuramochi[1,2,3], Satoshi Takeuchi[1,2*†], Hironari Kamikubo[4], Mikio Kataoka[4], Tahei Tahara[1,2*]

We report fifth-order time-domain Raman spectroscopy of photoactive yellow protein (PYP), with the aim to visualize vibrational coupling in its excited state. After the ultrashort actinic pump pulse prepared the vibrational coherence and population in the excited state, the evolving vibrational structure was tracked by time-resolved impulsive stimulated Raman spectroscopy using sub–7-fs pulses. The obtained fifth-order time-domain Raman data were translated to a two-dimensional (2D) frequency-frequency correlation map, which visualizes the correlation between low- and high-frequency vibrational modes of the excited state. The 2D map of PYP reveals a cross peak, indicating the coupling between the phenolic C–O stretch mode of the chromophore and the low-frequency modes (~160 cm^{-1}), assignable to the intermolecular motions involving the surrounding hydrogen-bonded amino acids. The unveiled coupling suggests the importance of the low-frequency vibrational motion in the primary photoreaction of PYP, highlighting the unique capability of this spectroscopic approach for studying ultrafast reaction dynamics.

INTRODUCTION

Chemical reactions proceed with nuclear rearrangements, which are described by the reaction coordinate represented on the corresponding potential energy surface (PES). The PES for polyatomic systems involves a vast degree of freedom of nuclear coordinates and hence is very complex. For unraveling (and manipulating) the reaction coordinate and molecular mechanisms that underlie the reaction, it is desirable to map out the PES, which has been a long-lasting central subject in both experimental and theoretical studies. In this quest, understanding of the vibrational coupling between normal mode coordinates is essential because it actually characterizes the complex shape of the PES. In particular, the vibrational coupling of low-frequency modes has attracted a tremendous interest. Low-frequency modes act as an energy acceptor in vibrational energy relaxation processes, and thus, their coupling is essential for the energy flow in the vibrational manifold. In addition, some particular low-frequency modes in biological systems, such as hydrogen bond vibrational modes and protein phonon modes, have been proposed to play an important role in directing biochemical reactions to achieve high functionality and/or selectivity, pointing to the importance of the vibrational coupling with the low-frequency modes (*1*–*3*). Disentangling how these low-frequency modes couple with other high-frequency fingerprint vibrations provides a wealth of information about the PESs, which is expected to bring about deeper insights into the reaction dynamics of polyatomic molecules.

Multidimensional vibrational spectroscopy has the capability to unravel vibrational couplings with high time and frequency resolution (*4*, *5*). In particular, two-dimensional infrared spectroscopy (2D-IR) has been extensively developed in the past decades (*6*) and has been successfully used for studying the vibrational coupling, anharmonicity, and dynamics of liquids and biological molecules (*7*–*11*). However, its application to low-frequency vibrational modes (<1000 cm^{-1}) has been challenging because of the lack of intense femtosecond light sources to implement 2D-IR experiments in this frequency range. On the other hand, multidimensional Raman spectroscopy is, in principle, capable of tackling this problem (*12*), but the application of this high-order nonlinear spectroscopic technique is not straightforward because of the interference from cascaded third-order nonlinear processes (*13*, *14*).

Recently, we studied excited-state proton transfer dynamics of green fluorescent protein (GFP) by using time-resolved impulsive stimulated Raman spectroscopy (TR-ISRS) (*15*). In TR-ISRS, temporal evolution of transient vibrational structure can be tracked on the femtosecond time scale through the observation of coherent nuclear wave packet motions in the time domain (*16*–*21*). In this previous study, we found that one of the high-frequency transient Raman bands of excited-state GFP showed a substantial intensity oscillation in the time domain with a frequency as low as 105 cm^{-1}. This observation was attributed to the anharmonic coupling of the high-frequency mode with the 105-cm^{-1} mode that is coherently excited within the bandwidth of the actinic pump pulse. Although the pulse duration of the actinic pump used in the previous study (~100 fs) was not short enough to generate vibrational coherence beyond ~200 cm^{-1}, these results strongly indicated a high potential of TR-ISRS to reveal vibrational couplings between the high- and low-frequency vibrational modes in reactive excited states.

Here, we report TR-ISRS measurements using an ultrashort actinic pump pulse and sub–7-fs Raman pump/probe pulses, with the aim to develop a new spectroscopic scheme to interrogate and visualize the vibrational coupling in the reactive excited state. By exploiting the 35-fs actinic pump pulse to coherently excite vibrational modes of the excited state up to ~1000 cm^{-1}, this fifth-order time-domain Raman approach allows us to draw a 2D Raman frequency-frequency correlation map with wide excitation and detection frequency windows. The model system investigated here is a bacterial blue light photoreceptor called photoactive yellow protein (PYP). The function of this protein is realized through a photocycle (*22*, *23*), and it is driven by the ultrafast trans-to-cis photoisomerization of the embedded chromophore,

[1]Molecular Spectroscopy Laboratory, RIKEN, 2-1 Hirosawa, Wako 351-0198, Japan. [2]Ultrafast Spectroscopy Research Team, RIKEN Center for Advanced Photonics (RAP), 2-1 Hirosawa, Wako 351-0198, Japan. [3]PRESTO, Japan Science and Technology Agency, 4-1-8 Honcho, Kawaguchi 332-0012, Japan. [4]Graduate School of Materials Science, Nara Institute of Science and Technology, 8916-5 Takayama, Ikoma, Nara 630-0192, Japan.
*Corresponding author. Email: stake@riken.jp (S.T.); tahei@riken.jp (T.T.)
†Present address: Graduate School of Material Science, University of Hyogo, 3-2-1 Kohto, Kamigori, Hyogo 678-1297, Japan.

p-coumaric acid (pCA), that is anchored by hydrogen bonds with the surrounding amino acid residues (Fig. 1) (*24*). It was previously shown that the mutation of an amino acid residue surrounding pCA substantially changes its excited-state lifetime and the low-frequency (inter- and intramolecular) vibrational structure (*25*, *26*), suggesting that the low-frequency vibrations play a key role to realize the efficient entry into the photocycle. In addition, our previous TR-ISRS study found that a low-frequency mode containing intermolecular vibrational character in excited-state PYP at 135 cm^{-1}, a chromophore vibration coupled with the motion of the hydrogen-bonded amino acid residues (Tyr42 and Glu46), shows distinct dynamics within 1 ps after photoexcitation, indicating the ultrafast change in the hydrogen bond structure around the chromophore. Because pCA is anchored by these hydrogen bonds in the protein pocket, one expects that the low-frequency intermolecular vibration modulates this geometrical constraint and affects the isomerization dynamics. Therefore, it is of particular interest to clarify how such an intermolecular vibrational mode is coupled with other key skeletal vibrational modes that are sensitive to the isomerization. In this sense, PYP is the most intriguing system to explore with the present fifth-order time-domain Raman spectroscopy, which is expected to reveal the importance of the vibrational coupling with low-frequency modes in the biological system. The present study successfully reveals the existence of vibrational couplings between low- and high-frequency vibrational modes of excited-state PYP and demonstrates the potential of the fifth-order time-domain Raman spectroscopy to map out the potential energy landscape of the reactive excited states.

RESULTS AND DISCUSSION

The experimental scheme of the present measurement is illustrated in Fig. 2A. The actinic pump pulse (P_1, 35 fs) prepares the excited-state (S_1) population and the coherent nuclear wave packet motion along the Raman-active low-frequency modes (<1000 cm^{-1}) of the excited state. Delayed from the P_1 pulse by a variable delay time ΔT, the second, ultrashort impulsive Raman pump pulse (P_2, <7 fs) is introduced to induce coherent nuclear motion in the excited state along all the Raman-active modes coupled to the electronic transition ($S_1 \rightarrow S_0$). The resultant nuclear wave packet motion is monitored by scanning the delay τ of the third, ultrashort probe pulse (P_3, <7 fs) with respect to the P_2 pulse and is observed as oscillatory features of the P_2-induced differential absorption signal. The vibrational coherence induced by the P_2 pulse carries the structural information of the transient at ΔT after the start of the photoreaction by the P_1 pulse. Moreover, the P_2-induced coherence, which is generated during the free induction decay of the P_1-induced vibrational coherence, carries information about the coupling between the vibrational modes that are coherently excited at the two different timings ($\Delta T = 0$ and $\tau = 0$).

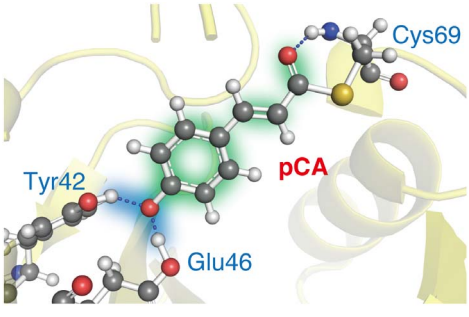

Fig. 1. Structure of the chromophore pocket in PYP. Structure of trans-pCA chromophore of PYP. Blue dotted lines denote hydrogen bonds with the surrounding amino acid residues. Vibrational couplings between low-frequency modes involving intermolecular motions through the hydrogen bonds (blue shaded) and fingerprint vibrations reflecting the pCA skeleton (green shaded) are of particular interest in the present study.

The red curve in Fig. 2B shows a pump-probe signal of PYP in a tris-HCl buffer solution (pH 7), which was measured with the 35-fs actinic pump pulse (P_1, 450 nm) and sub–7-fs probe pulse (P_3, 500 to 680 nm). This pump-probe signal monitors the decay of the stimulated emission signal that appears in the spectral region of the probe pulse (see the Supplementary Materials for the spectral condition of the measurement). The coherent nuclear wave packet motion in the excited state, which is induced by the P_1 pulse, is recognized as the oscillatory feature of the signal. Fourier transform analysis of this oscillatory component, which was extracted by subtracting the slowly varying population dynamics, provides the vibrational spectrum of the Franck-Condon state up to ~1000 cm^{-1} (Fig. 2C, top). This P_1-induced vibrational spectrum nicely agrees with that we previously reported (*21*). Under this actinic pumping condition, the sub–7-fs impulsive Raman pump pulse (P_2, 500 to 680 nm) was introduced at, e.g., $\Delta T = 0.5$ ps. As shown by the blue curve in Fig. 2B, the P_2 pulse induces the depletion of the excited-state population through the stimulated emission transition, as well as the substantial oscillatory feature, because of the coherent nuclear wave packet motion in the excited state. Fourier transform analysis of this P_2-induced oscillatory component along the τ axis yields a snapshot vibrational spectrum of excited-state PYP in the presence of the P_1-induced vibrational coherence (Fig. 2C, bottom). In this way, the P_2-induced oscillatory signals were measured at various ΔT delay times (Fig. 3A), and a series of femtosecond time-resolved Raman spectra of excited-state PYP were obtained, as shown in Fig. 3B.

The obtained femtosecond time-resolved Raman spectra exhibit a number of vibrational bands of excited-state PYP. Peak frequencies of the observed bands (135, 262, 311, 432, 538, 751, and 1160 cm^{-1}) are in good agreement with those found in our previous TR-ISRS study of PYP (*21*). However, the intensity patterns of the obtained spectra are very different from that which we previously reported. We find that most of the bands show a substantial intensity oscillation against the ΔT delay time. This oscillatory feature is more readily seen in the 2D Fourier amplitude map shown in Fig. 3C, in which the amplitude recurrence is clearly recognized for many bands. Temporal profiles of the Fourier amplitude for the selected bands are shown in Fig. 4. All the presented bands show a substantial oscillatory feature along the ΔT delay time. We fitted these temporal profiles with a sum of exponential and damped cosine functions, convoluted with the instrumental response. The best-fit curves are shown in Fig. 4 with dashed lines. From this analysis, we find that most of the bands show the amplitude oscillation at their own vibrational frequencies. For example, the band at 135 cm^{-1} shows the amplitude oscillation with an ~247-fs period (~135 cm^{-1}), and the band at 311 cm^{-1} shows the amplitude oscillation with an ~107-fs period (~311 cm^{-1}). We note that the 751-cm^{-1} band shows the oscillation frequency that looks different from its own vibrational frequency because of the undersampling, but the observed oscillatory feature actually corresponds to 751 cm^{-1} (see the following sections for details). Because these oscillatory features were not observed in the previous TR-ISRS study of PYP performed with the 290-fs P_1 pulse (*21*), the oscillatory feature should arise from the coherent nuclear wave packet motion that is induced by the ultrashort P_1 pulse (35 fs) used in the present study.

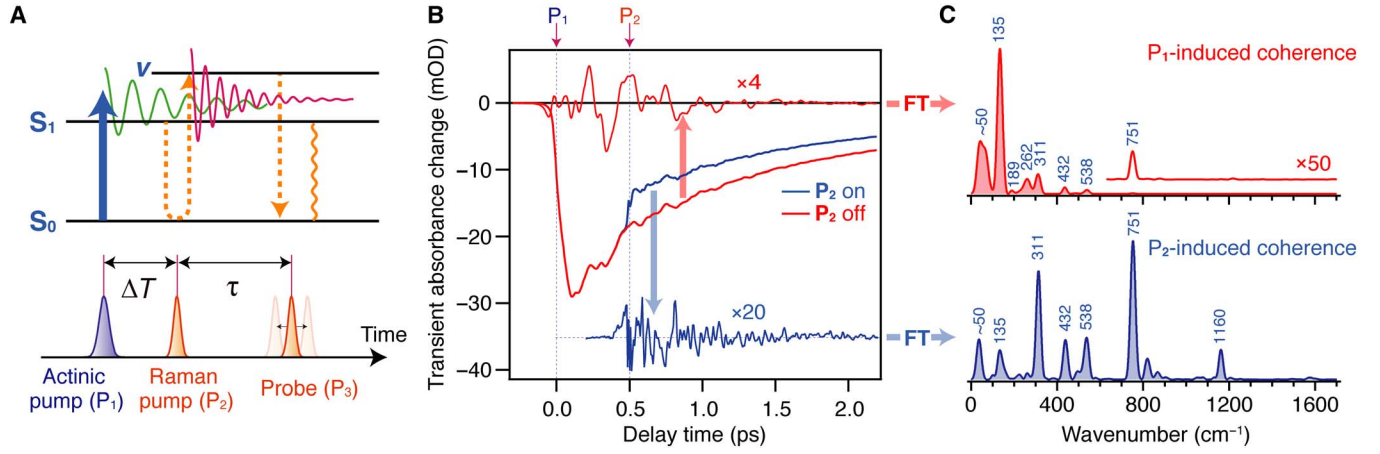

Fig. 2. Principle of the fifth-order time-domain Raman spectroscopy of PYP. (**A**) Schematic illustration of the optical process involved in the present fifth-order time-domain Raman measurement. (**B**) Pump-probe signals of PYP in a tris-HCl buffer solution (pH 7), which were measured with (blue) and without (red) the P_2 pulse at ΔT = 0.5 ps. The raw TR-ISRS signal was obtained as a difference between these signals (i.e., P_2 on − P_2 off). P_1-induced (red) and P_2-induced (blue) oscillatory signals were obtained after subtraction of the slowly varying population component from the raw signals, and they are shown with magnification (×4 and ×20, respectively). (**C**) Fourier transform (FT) power spectra of the P_1- and P_2-induced oscillatory signals.

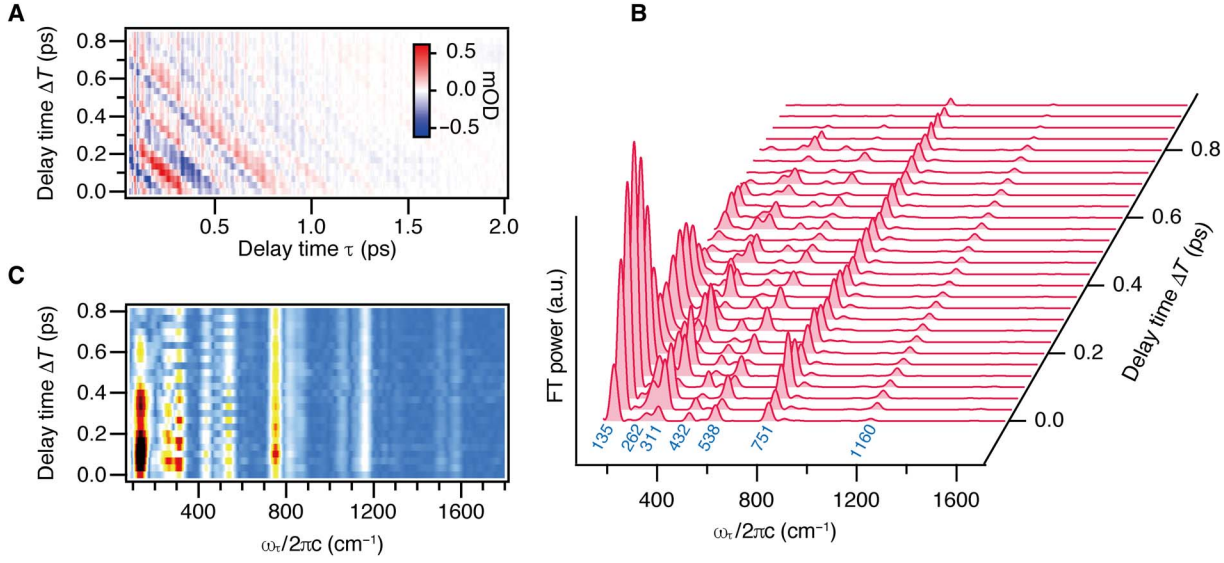

Fig. 3. Fifth-order time-domain Raman data of PYP. (**A**) 2D representation of the P_2-induced oscillatory signals obtained at various ΔT delay times. (**B**) Fourier transform power spectra of the oscillatory signals obtained at various ΔT delay times. (**C**) 2D representation of the time-resolved Fourier amplitude spectra.

To closely analyze and visualize these oscillatory features, we constructed a 2D frequency-frequency correlation map by performing Fourier transform of the 2D Fourier amplitude data (Fig. 3C) along the ΔT axis after subtracting the exponentially decaying component. The obtained 2D frequency-frequency correlation map is shown in Fig. 5. A number of peaks are recognized in the 2D map, which indicates the correlation between the two vibrational coherences: One is the coherence induced by the P_1 pulse at ΔT = 0 ps, and the other is that induced by the P_2 pulse at τ = 0 ps. All the observed peaks are vertically elongated because the frequency resolution in the $\omega_{\Delta T}$ axis is lower as a result of the shorter scanning range for the ΔT delay (800 fs) than that for the τ delay (2 ps). In the 2D map, the most prominent feature is the intense diagonal peaks that represent the amplitude oscillation of the bands at their own vibrational frequencies against ΔT, as presented in Fig. 4. The peaks on the antidiagonal line (blue dotted) also correspond to the diagonal peaks that are folded as a result of the undersampling along the ΔT axis; any oscillations at frequencies ($\omega_{\Delta T}$) above the Nyquist frequency ω_{Nq} (500 cm^{-1}) appear at $2\omega_{Nq} - \omega_{\Delta T}$ cm^{-1} under the present experimental condition. In addition to these diagonal (and antidiagonal) peaks, several off-diagonal (cross) peaks appear in the 2D correlation map, representing the coupling between different vibrational modes.

First, we discuss the origin of the diagonal peaks, that is, the amplitude oscillation of the vibrational coherence at its own frequency. In general, the overall optical process involved in the present experiment is treated as $\chi^{(5)}$ processes because the time-domain Raman probing is performed while the P_1-induced vibrational coherence remains. Within this framework, the diagonal peaks are interpreted as depletion of the P_1-induced vibrational coherence by the interaction with the P_2 pulse. Previously, Fujiyoshi *et al.* (*27*) examined the contribution of the $\chi^{(5)}$

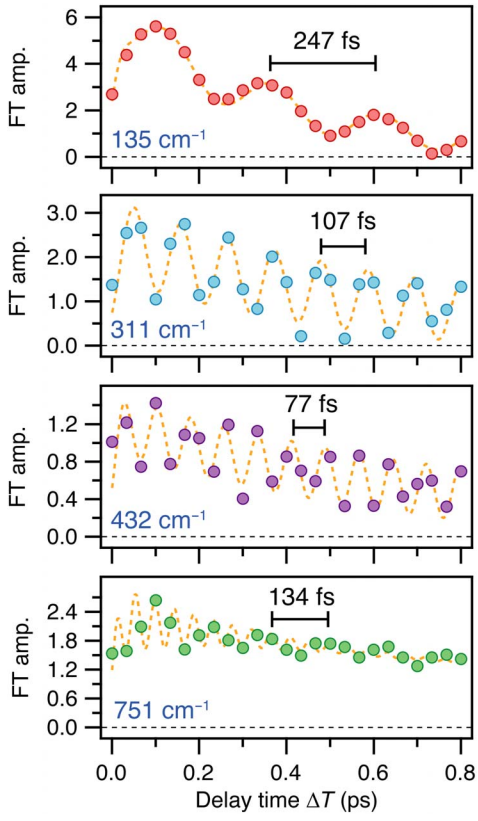

Fig. 4. Temporal change of the Raman band intensities of excited-state PYP. Temporal profiles of the Fourier amplitude for selected bands. Dashed lines denote the best fit to the data, which takes account of the oscillatory component with slowly varying population component.

processes in the TR-ISRS data measured with the ultrashort P_1 pulse. They pointed out that the vibrational coherence in the excited state prepared by the P_1 pulse can be depleted by the P_2 pulse because of the coherence transfer to other vibrational modes or the population transfer to a different electronic state. This depletion [$\chi^{(5)}$] signal appears in the raw TR-ISRS data because it is also the P_2-induced differential signal that is experimentally recorded (see the Supplementary Materials for typical energy ladder diagrams responsible for this coherence depletion). Thus, the oscillatory component of the total P_2-induced differential absorption signal for a vibrational mode with frequency ν is represented as

$$\Delta A_{\mathrm{total}}(\Delta T,\tau)=\left\{A^0_{\mathrm{P2}}\cos(2\pi\nu\tau)\exp\left(-\frac{\Delta T}{T_{\mathrm{S1}}}\right)-\right.$$

$$\left.\eta A^0_{\mathrm{P1}}\exp\left(-\frac{\Delta T}{T_\nu}\right)\cos(2\pi\nu\tau+\theta(\Delta T))\right\}\exp\left(-\frac{\tau}{T_\nu}\right) \quad (1)$$

where $\theta(\Delta T)=2\pi\nu\Delta T$ and where A^0_{P1} and A^0_{P2}, ν, T_ν, η, and T_{S1} represent the oscillation amplitude of the P_1- and P_2-induced vibrational coherences, vibrational frequency, vibrational dephasing time, depletion efficiency of the P_1-induced coherence by the P_2 pulse, and lifetime of the excited state (S_1), respectively. The first term in Eq. 1 represents a vibrational coherence newly created by the P_2 pulse, whereas the second term denotes the depletion of the vibrational coherence generated by the preceding P_1 pulse (see the Supplementary Materials for the formulation). The phase $\theta(\Delta T)$ (and amplitude) of the latter depletion signal (the second term) depends on the ΔT delay time, and thus, it can constructively or destructively interfere with the P_2-induced coherence (the first term). The sum of the two terms represents the oscillatory feature of the Fourier amplitude against the ΔT delay time, as observed for the bands shown in

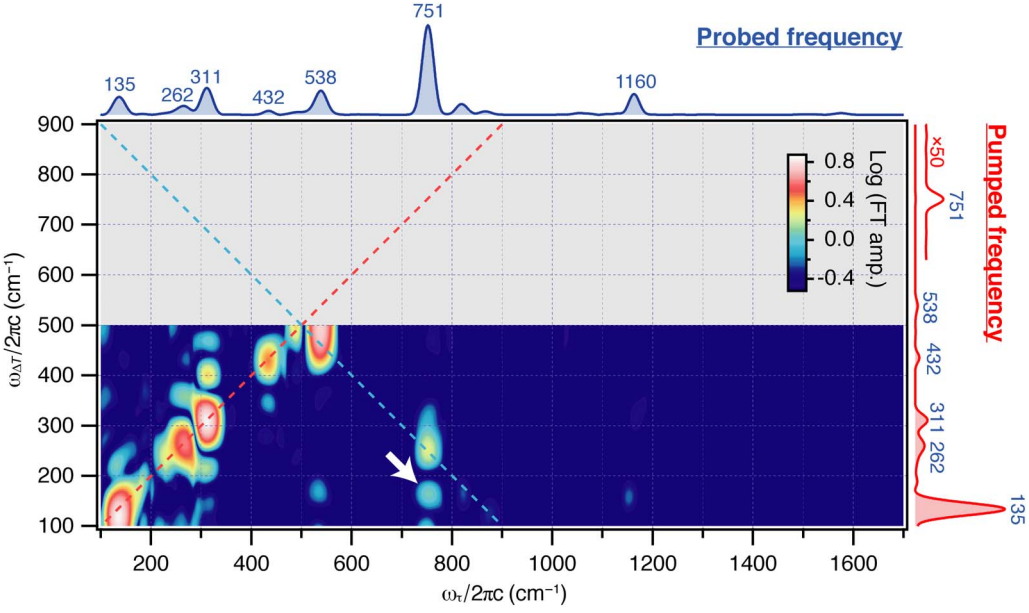

Fig. 5. 2D representation of the fifth-order time-domain Raman data. 2D frequency-frequency correlation map obtained by the fifth-order time-domain Raman spectroscopy of PYP. Top half of the 2D map (gray-shaded area) was not directly obtained because of the undersampling in the ΔT axis but is folded to the lower half. Diagonal peaks on the red broken line correspond to the depletion of P_1-induced vibrational coherence. Off-diagonal peaks on the blue broken line correspond to the folded diagonal peaks that appear as a result of the undersampling. Spectra on the top and right represent the Fourier transform power spectrum of the oscillatory component of the TR-ISRS signal, averaged over all the measured ΔT delays, and that of the pump-probe signal, respectively, the latter of which is the same as Fig. 2C.

Fig. 4. This gives rise to the diagonal peaks as found in the 2D map in Fig. 5. Therefore, the diagonal peaks predominantly carry the information on the P_1-induced vibrational coherence, although detailed analysis of their shapes, in principle, has potential to provide more information, for example, on the broadening mechanism of each vibrational band.

In contrast to the diagonal peaks, cross peaks contain irreplaceable information about the coupling among vibrational modes. In the 2D map obtained in this study, the most pronounced cross peak is seen between $\omega_\tau = 751$ cm^{-1} and $\omega_{\Delta T} = \sim 160$ cm^{-1}, as indicated by an arrow in Fig. 5, and another prominent cross peak is also recognized for $\omega_\tau = 538$ cm^{-1} and $\omega_{\Delta T} = \sim 160$ cm^{-1}. These cross peaks represent coupling between the two frequency components. To further confirm the existence of the cross peak, we performed a TR-ISRS measurement by using the 75-fs P_1 pulse that has a 400-cm^{-1} bandwidth (full width at the half maximum). This pulse duration (bandwidth) was carefully chosen so that the P_1 pulse does not coherently excite vibrational modes above ~600 cm^{-1} and hence suppresses the oscillatory component because of the depletion of the P_1-induced vibrational coherence for the 751-cm^{-1} mode. Simultaneously, this pulse duration limits the coupling partner to vibrational modes below ~600 cm^{-1}, negating a possible coupling with (undersampled) higher-frequency modes. Consequently, we can selectively observe and examine the oscillation due to the coupling between the 751- and ~160-cm^{-1} modes directly in the time domain. It is difficult to further stretch the P_1 pulse duration because it lowers the efficiency to coherently excite low-frequency modes. Thus, we cannot sufficiently suppress the P_1-induced vibrational coherence for the 538-cm^{-1} mode. Accordingly, we focus on the cross peak between the 751- and ~160-cm^{-1} vibrations hereafter and do not further discuss the cross peak observed between the 538- and ~160-cm^{-1} vibrations.

In Fig. 6A, a pump-probe signal of PYP obtained by the 75-fs pump pulse is shown. The signal shows the oscillatory feature that is dominated by the low-frequency vibrations at ~50 and 135 cm^{-1}, as indicated by its Fourier transform shown in Fig. 6B. Under this actinic pumping condition, TR-ISRS measurements were carried out, and the obtained temporal profile of the Fourier amplitude of the 751-cm^{-1} band is shown in Fig. 6C. The data clearly show that the Fourier amplitude of the 751-cm^{-1} band exhibits an unambiguous oscillatory feature against ΔT, confirming that the 751-cm^{-1} band intensity is certainly modulated by the P_1-induced coherent low-frequency motion as represented by the cross peak in the 2D map.

The amplitude oscillation of the 751-cm^{-1} band is attributable to the periodic modulation of the displacement between the S_1 and S_0 PESs along the corresponding nuclear coordinate through the anharmonic coupling with the low-frequency modes [detailed discussion on this picture is given in the Supporting Information of (*15*)]. Fourier analysis of the oscillatory feature showed a broad peak at around 180 cm^{-1} (Fig. 6D), which most likely originates from the mixed contribution from the 135- and 189-cm^{-1} modes that appear in the pump-probe data (Fig. 6B). Although the 189-cm^{-1} mode is very weak in the Franck-Condon vibrational spectrum obtained with the pump-probe spectroscopy, its contribution appears very pronounced in the amplitude oscillation of the 751-cm^{-1} band, suggesting strong vibrational coupling between these modes. This result demonstrates the unique capability of the present fifth-order time-domain Raman spectroscopy to exclusively probe the pairs of coupled vibrational modes, thereby sensitively reporting the distortion of the PESs through the anharmonic coupling. This information is essential for mapping complex, reactive PESs but is barely available with conventional third-order nonlinear spectroscopies

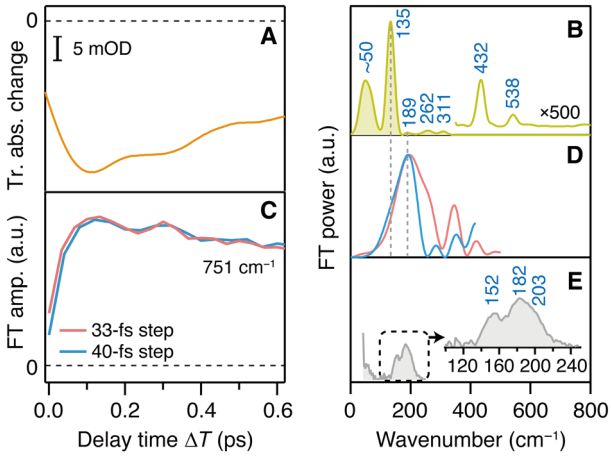

Fig. 6. Low-frequency oscillatory dynamics of the high-frequency fingerprint vibrational mode. (**A**) Pump-probe signal of PYP in the early time window, measured with 75-fs pump and 6.5-fs probe pulses. (**B**) Fourier transform power spectrum of the oscillatory component of the pump-probe signal in (A). (**C**) Temporal profile of the Fourier amplitude of the 751-cm^{-1} band of excited-state PYP obtained by TR-ISRS using the 75-fs P_1 pulse. Red and blue lines represent the data measured with the different ΔT step sizes. The data taken with the different ΔT steps confirm that the oscillatory feature of the 751-cm^{-1} band is not undersampled. (**D**) Fourier transform power spectra of the amplitude oscillation of the 751-cm^{-1} band in (C). (**E**) Steady-state preresonance stimulated Raman spectrum of the ground-state PYP, obtained with 490-nm Raman excitation.

such as pump-probe spectroscopy. This is because coherent nuclear wave packet motion is observed regardless of whether the relevant mode is anharmonic or not in these techniques.

On the basis of the previous steady-state resonance Raman and TR-ISRS studies for wild-type PYP and various mutants (*21*, *25*), the 135-cm^{-1} mode has been assigned to a chromophore vibration coupled to the intermolecular motion with the hydrogen-bonded amino acid residues (Tyr42 and Glu46). The assignment of the 189-cm^{-1} mode is not clear; however, we consider that this mode also has an intermolecular vibrational character because the spectral feature of its counterpart in the S_0 state (182 or 203 cm^{-1}; Fig. 6E) was shown to be highly sensitive to the mutation of the surrounding amino acid residues (*25*). On the other hand, the 751-cm^{-1} mode could be assigned to the phenolic C—O stretch mode of pCA (coupled with the C_{ph}-C_{et} stretch and C=O bend) by comparison with the previous steady-state Raman data (*28*). Because this phenolic oxygen site is directly hydrogen-bonded to the two amino acid residues (Tyr42 and Glu46), it is highly likely that the intermolecular low-frequency vibrations at the phenolic tail part of pCA distort the PES along the phenolic C—O stretch coordinate through the anharmonic coupling, which gives rise to the pronounced cross peak in the 2D frequency-frequency correlation map.

It is intriguing whether the observed coupling plays any roles in the isomerization reaction of pCA that drives the photocycle of PYP. The isomerization of pCA has been considered to proceed in a volume-conserving manner (i.e., hula-twist and/or bicycle-pedal) because of the geometric constraint by the packed protein environment, as well as the anchoring by the hydrogen bonds at the phenolic tail part (*29*). Because these isomerization mechanisms require some nuclear motions around the phenolic tail part of pCA, the observed coupling between the phenolic C—O stretch (751 cm^{-1}) and low-frequency intermolecular vibrational modes (135 and 189 cm^{-1}) may affect the trans-to-cis isomerization dynamics, i.e., the twisting of the C_{et}=C_{et} double bond. In other words,

modulation of the hydrogen bond strength at the phenolic tail part by the low-frequency modes temporarily relaxes the geometric constraint of pCA, which might facilitate the rotation around the C_{et}=C_{et} double bond, as proposed previously (*30*). To provide a clear answer to this question, it is desirable to examine the correlation between the low-frequency modes and the key C_{et}=C_{et} stretch mode. Unfortunately, however, this is a difficult task under the present experimental condition because the resonance Raman activity of the C_{et}=C_{et} stretch mode is very low and the corresponding band is not clearly observed (Fig. 3B). Nevertheless, fifth-order time-domain Raman experiments using other electronic transitions [e.g., $S_n \leftarrow S_1$ transition in the ultraviolet region (*21*, *31*)] for the P_2 and P_3 pulses may enable direct visualization of the correlation between the isomerization coordinate and low-frequency intermolecular vibrational modes, which would significantly advance our understanding of the PES that governs the primary process of the PYP photoreaction.

CONCLUSION

In summary, we have performed the fifth-order time-domain Raman spectroscopy of PYP. The TR-ISRS data acquired with the 35-fs P_1 pulse allowed us to obtain the 2D frequency-frequency correlation map that can visualize couplings among vibrational modes in the excited state. The obtained 2D data of PYP exhibit the diagonal peaks originating from the depletion of the P_1-induced vibrational coherence; however, the cross peak between the low-frequency intermolecular vibrations and the 751-cm^{-1} phenolic C—O stretch vibration was clearly observed, manifesting the vibrational coupling between these modes. The observed vibrational coupling implies the possibility that the low-frequency intermolecular vibration alleviates the geometric constraint of pCA and thus facilitates the isomerization.

By virtue of the resonance enhancement using two different electronic transitions, i.e., $S_1 \leftarrow S_0$ absorption and $S_1 \rightarrow S_0$ stimulated emission transitions, the present time-domain Raman approach can circumvent the cascading of the third-order processes, which has been a technical bottleneck to implement 2D Raman spectroscopy (*13*, *14*, *32*–*35*). From this perspective, our approach has technical similarity to 4D electronic Raman and 2D resonance Raman spectroscopies, which were developed recently (*36*, *37*). On the other hand, our technique is specific and dedicated to observing vibrational coupling in the excited state, which is achieved by using electronic transitions exclusive to the excited-state molecule in the six-wave mixing process. In this sense, the present technique shares an experimental concept with the frequency-domain approach, i.e., 2D femtosecond stimulated Raman spectroscopy (*38*), and hence can be called 2D impulsive stimulated Raman spectroscopy (2D-ISRS). Our time-domain approach is complementary to the frequency-domain approach, yet the implementation of the time-domain Raman probing offers a wider detection frequency window (including the low-frequency terahertz region), which allows us to fully characterize vibrational couplings. The present study demonstrates the potential of the fifth-order time-domain Raman approach to clarify the vibrational coupling in reactive excited states, and we envisage that this new approach will provide a wealth of insights into the role of low-frequency vibrational motions in mediating various chemical reactions.

MATERIALS AND METHODS

Sample preparation

Wild-type PYP was prepared as described previously (*39*). The sample was dissolved in 10 mM tris-HCl buffer at pH 7. The typical concentration of the sample solutions was ~300 μM. Sample degradation was examined by measuring the absorption spectrum of the solution immediately before and after each measurement. The change in the optical purity index [optical density (OD) at 277 nm/OD at 446 nm] after each measurement was less than 5%.

TR-ISRS measurements (fifth-order time-domain Raman spectroscopy)

Details of our TR-ISRS spectrometer were described in detail elsewhere (*20*). Briefly, the setup is based on two home-built noncollinear optical parametric amplifiers (NOPAs) that are driven by the output of the Ti:sapphire regenerative amplifier (780 nm, 80 fs, 1 mJ, 1 kHz). The first NOPA generates the actinic pump pulse (P_1) at 450 nm, which was compressed down to 35 fs. For the experiment with the longer P_1 pulse duration, the compressed output was spectrally filtered by a grating-based 4f setup to stretch the pulse to 75 fs. The second NOPA generates a broadband ultrashort pulse (500 to 680 nm, 6.5 fs). This 6.5-fs pulse was divided into two, and they were used as the impulsive Raman pump pulse (P_2) and probe pulse (P_3) to monitor the transient absorbance change. A small fraction of the P_3 pulse was picked up and used as the reference pulse. The P_1, P_2, and P_3 pulses were focused into a 300-μm-thick flow cell of the sample solution. At the sample position, the energies of the P_1, P_2, and P_3 pulses were typically 80, 70, and 6 nJ, respectively, and their polarizations were set parallel. The intensities of the probe and reference pulses were detected by photodiodes, and the signals were processed on a shot-to-shot basis to evaluate the P_2-induced differential absorbance by mechanically chopping every other P_2 pulse.

SUPPLEMENTARY MATERIALS

Supplementary material for this article is available at http://advances.sciencemag.org/cgi/content/full/5/6/eaau4490/DC1

Experimental condition

Origin of the diagonal peaks in the 2D frequency-frequency correlation map

Fifth-order signal versus lower-order cascades

Fig. S1. Resonance condition for the measurements.

Fig. S2. Depletion of vibrational coherence in the TR-ISRS experiment.

REFERENCES AND NOTES

1. J. Deàk, H.-L. Chiu, C. M. Lewis, R. J. D. Miller, Ultrafast phase grating studies of heme proteins: Observation of the low-frequency modes directing functionally important protein motions. *J. Phys. Chem. B* **102**, 6621–6634 (1998).
2. D. Liu, X. Q. Chu, M. Lagi, Y. Zhang, E. Fratini, P. Baglioni, A. Alatas, A. Said, E. Alp, S. H. Chen, Studies of phononlike low-energy excitations of protein molecules by inelastic x-ray scattering. *Phys. Rev. Lett.* **101**, 135501 (2008).
3. D. A. Turton, H. M. Senn, T. Harwood, A. J. Lapthorn, E. M. Ellis, K. Wynne, Terahertz underdamped vibrational motion governs protein-ligand binding in solution. *Nat. Commun.* **5**, 3999 (2014).
4. S. Mukamel, *Principles of Nonlinear Optical Spectroscopy* (Oxford Univ. Press, 1995), vol. 6, pp. 543 pp.
5. S. Mukamel, Multidimensional femtosecond correlation spectroscopies of electronic and vibrational excitations. *Annu. Rev. Phys. Chem.* **51**, 691–729 (2000).
6. P. Hamm, M. T. Zanni, *Concepts and Methods of 2D Infrared Spectroscopy* (Cambridge Univ. Press, 2011).
7. P. Hamm, J. Helbing, J. Bredenbeck, Two-dimensional infrared spectroscopy of photoswitchable peptides. *Annu. Rev. Phys. Chem.* **59**, 291–317 (2008).
8. S. T. Roberts, K. Ramasesha, A. Tokmakoff, Structural rearrangements in water viewed through two-dimensional infrared spectroscopy. *Acc. Chem. Res.* **42**, 1239–1249 (2009).
9. T. Elsaesser, Two-dimensional infrared spectroscopy of intermolecular hydrogen bonds in the condensed phase. *Acc. Chem. Res.* **42**, 1220–1228 (2009).
10. M. D. Fayer, D. E. Moilanen, D. Wong, D. E. Rosenfeld, E. E. Fenn, S. Park, Water dynamics in salt solutions studied with ultrafast two-dimensional infrared (2D IR) vibrational echo spectroscopy. *Acc. Chem. Res.* **42**, 1210–1219 (2009).

11. N. T. Hunt, 2D-IR spectroscopy: Ultrafast insights into biomolecule structure and function. *Chem. Soc. Rev.* **38**, 1837–1848 (2009).
12. Y. Tanimura, S. Mukamel, Two-dimensional femtosecond vibrational spectroscopy of liquids. *J. Chem. Phys.* **99**, 9496–9511 (1993).
13. D. J. Ulness, J. C. Kirkwood, A. C. Albrecht, Competitive events in fifth order time resolved coherent Raman scattering: Direct versus sequential processes. *J. Chem. Phys.* **108**, 3897–3902 (1998).
14. D. A. Blank, L. J. Kaufman, G. R. Fleming, Fifth-order two-dimensional Raman spectra of CS_2 are dominated by third-order cascades. *J. Chem. Phys.* **111**, 3105–3114 (1999).
15. T. Fujisawa, H. Kuramochi, H. Hosoi, S. Takeuchi, T. Tahara, Role of coherent low-frequency motion in excited-state proton transfer of green fluorescent protein studied by time-resolved impulsive stimulated Raman spectroscopy. *J. Am. Chem. Soc.* **138**, 3942–3945 (2016).
16. S. Fujiyoshi, S. Takeuchi, T. Tahara, Time-resolved impulsive stimulated Raman scattering from excited-state polyatomic molecules in solution. *J. Phys. Chem. A* **107**, 494–500 (2003).
17. G. Cerullo, L. Lüer, C. Manzoni, S. de Silvestri, O. Shoshana, S. Ruhman, Time domain investigation of excited-state vibrational motion in organic molecules by stimulated emission pumping. *J. Phys. Chem. A* **107**, 8339–8344 (2003).
18. S. Takeuchi, S. Ruhman, T. Tsuneda, M. Chiba, T. Taketsugu, T. Tahara, Spectroscopic tracking of structural evolution in ultrafast stilbene photoisomerization. *Science* **322**, 1073–1077 (2008).
19. J. P. Kraack, A. Wand, T. Buckup, M. Motzkus, S. Ruhman, Mapping multidimensional excited state dynamics using pump-impulsive-vibrational-spectroscopy and pump-degenerate-four-wave-mixing. *Phys. Chem. Chem. Phys.* **15**, 14487–14501 (2013).
20. H. Kuramochi, S. Takeuchi, T. Tahara, Femtosecond time-resolved impulsive stimulated Raman spectroscopy using sub-7-fs pulses: Apparatus and applications. *Rev. Sci. Instrum.* **87**, 043107 (2016).
21. H. Kuramochi, S. Takeuchi, K. Yonezawa, H. Kamikubo, M. Kataoka, T. Tahara, Probing the early stages of photoreception in photoactive yellow protein with ultrafast time-domain Raman spectroscopy. *Nat. Chem.* **9**, 660–666 (2017).
22. T. E. Meyer, Isolation and characterization of soluble cytochromes, ferredoxins and other chromophoric proteins from the halophilic phototrophic bacterium *Ectothiorhodospira halophila*. *Biochim. Biophys. Acta* **806**, 175–183 (1985).
23. W. W. Sprenger, W. D. Hoff, J. P. Armitage, K. J. Hellingwerf, The eubacterium *Ectothiorhodospira halophila* is negatively phototactic, with a wavelength dependence that fits the absorption spectrum of the photoactive yellow protein. *J. Bacteriol.* **175**, 3096–3104 (1993).
24. K. J. Hellingwerf, J. Hendriks, T. Gensch, Photoactive yellow protein, a new type of photoreceptor protein: will this "yellow lab" bring us where we want to go? *J. Phys. Chem. A* **107**, 1082–1094 (2003).
25. H. Chosrowjan, S. Taniguchi, N. Mataga, M. Unno, S. Yamauchi, N. Hamada, M. Kumauchi, F. Tokunaga, Low-frequency vibrations and their role in ultrafast photoisomerization reaction dynamics of photoactive yellow protein. *J. Phys. Chem. B* **108**, 2686–2698 (2004).
26. P. Changenet-Barret, P. Plaza, M. M. Martin, H. Chosrowjan, S. Taniguchi, N. Mataga, Y. Imamoto, M. Kataoka, Structural effects on the ultrafast photoisomerization of photoactive yellow protein. transient absorption spectroscopy of two point mutants. *J. Phys. Chem. C* **113**, 11605–11613 (2009).
27. S. Fujiyoshi, T.-a. Ishibashi, H. Onishi, Fifth-order Raman spectroscopy of excited-state molecules. *J. Phys. Chem. A* **108**, 11165–11171 (2004).
28. M. Unno, M. Kumauchi, F. Tokunaga, S. Yamauchi, Vibrational assignment of the 4-hydroxycinnamyl chromophore in photoactive yellow protein. *J. Phys. Chem. B* **111**, 2719–2726 (2007).
29. Y. O. Jung, J. H. Lee, J. Kim, M. Schmidt, K. Moffat, V. Šrajer, H. Ihee, Volume-conserving trans–cis isomerization pathways in photoactive yellow protein visualized by picosecond x-ray crystallography. *Nat. Chem.* **5**, 212–220 (2013).
30. S. Yamaguchi, H. Kamikubo, K. Kurihara, R. Kuroki, N. Niimura, N. Shimizu, Y. Yamazaki, M. Kataoka, Low-barrier hydrogen bond in photoactive yellow protein. *Proc. Natl. Acad. Sci. U.S.A.* **106**, 440–444 (2009).
31. D. S. Larsen, I. H. M. van Stokkum, M. Vengris, M. A. van der Horst, F. L. de Weerd, K. J. Hellingwerf, R. van Grondelle, Incoherent manipulation of the photoactive yellow protein photocycle with dispersed pump-dump-probe spectroscopy. *Biophys. J.* **87**, 1858–1872 (2004).
32. A. Tokmakoff, M. J. Lang, D. S. Larsen, G. R. Fleming, V. Chernyak, S. Mukamel, Two-dimensional Raman spectroscopy of vibrational interactions in liquids. *Phys. Rev. Lett.* **79**, 2702–2705 (1997).
33. K. J. Kubarych, C. J. Milne, S. Lin, V. Astinov, R. J. D. Miller, Diffractive optics-based six-wave mixing: Heterodyne detection of the full $\chi^{(5)}$ tensor of liquid CS_2. *J. Chem. Phys.* **116**, 2016–2042 (2002).
34. L. J. Kaufman, J. Heo, L. D. Ziegler, G. R. Fleming, Heterodyne-detected fifth-order nonresonant Raman scattering from room temperature CS_2. *Phys. Rev. Lett.* **88**, 207402 (2002).
35. H. Frostig, T. Bayer, N. Dudovich, Y. C. Eldar, Y. Silberberg, Single-beam spectrally controlled two-dimensional Raman spectroscopy. *Nat. Photonics* **9**, 339–343 (2015).
36. B. P. Molesky, Z. Guo, T. P. Cheshire, A. M. Moran, Perspective: Two-dimensional resonance Raman spectroscopy. *J. Chem. Phys.* **145**, 180901 (2016).
37. E. Harel, Four-dimensional coherent electronic Raman spectroscopy. *J. Chem. Phys.* **146**, 154201 (2017).
38. D. P. Hoffman, S. R. Ellis, R. A. Mathies, Characterization of a conical intersection in a charge-transfer dimer with two-dimensional time-resolved stimulated Raman spectroscopy. *J. Phys. Chem. A* **118**, 4955–4965 (2014).
39. K. Mihara, O. Hisatomi, Y. Imamoto, M. Kataoka, F. Tokunaga, Functional expression and site-directed mutagenesis of photoactive yellow protein. *J. Biochem.* **121**, 876–880 (1997).

Acknowledgments

Funding: This work was partly supported by JSPS KAKENHI grant numbers JP16H04102 (to S.T.), JP25102003 (to H.Ka.), JP24247030 (to M.K.), and JP25104005 (to T.T.).
Author contributions: H.Ku., S.T., and T.T. conceived and designed the research. H.Ku. performed the experiment and analyzed the data. H.Ka. and M.K. expressed and purified the samples. H.Ku., S.T., and T.T. wrote the paper. All authors discussed the results and commented on the manuscript. **Competing interests:** The authors declare that they have no competing interests. **Data and materials availability:** All data needed to evaluate the conclusions in the paper are present in the paper and/or the Supplementary Materials. Additional data related to this paper may be requested from the authors.

Submitted 12 June 2018
Accepted 26 April 2019
Published 7 June 2019
10.1126/sciadv.aau4490

Citation: H. Kuramochi, S. Takeuchi, H. Kamikubo, M. Kataoka, T. Tahara, Fifth-order time-domain Raman spectroscopy of photoactive yellow protein for visualizing vibrational coupling in its excited state. *Sci. Adv.* **5**, eaau4490 (2019).

Fifth-order time-domain Raman spectroscopy of photoactive yellow protein for visualizing vibrational coupling in its excited state

Hikaru Kuramochi, Satoshi Takeuchi, Hironari Kamikubo, Mikio Kataoka and Tahei Tahara

Sci Adv **5** (6), eaau4490.
DOI: 10.1126/sciadv.aau4490